Supporting Information

A dense 3d-4f metal-organic framework with "gas pocket" for highly efficient CH_4/N_2 separation

Li-Min Zhu,[a] Wen-Liang Li,[a] Tian-Ran Li,[a] Lin-Ping Shi,[a] Li-Ting Li,[a] Zhao-Quan Yao,[a,*]Hong-Liang Huang,[b,*] Jiong-Peng Zhao[a,*] and Fu-Chen Liu[a,*]

Characterization

All of the materials for synthesis were obtained commercially and used without further purification. The powder X-ray diffraction (PXRD) data were characterized by using the Rigaku D/Max-2500 diffractometer with a Cu-target tube and a graphite monochromator (40 kV, 100 mA). Simulated PXRD pattern was derived from modulating the single-crystal X-ray diffraction (SCXRD) data via the Mercury software.

Thermogravimetric analysis was carried out on a GA Q50 TG-DTA analyzer from 25 to 800 °C in air atmosphere and the heating rate was 5 K/min. Brunauer-Emmett-Teller (BET) surface area was estimated by Ar adsorption-desorption isotherm measurements at 87 K recorded on Micromeritics ASAP 2020 PLUS HD88 instrument. Pore size distribution data were estimated based on the nonlocal density functional theory (NLDFT) method. The FTIR spectroscopies were obtained on the Bruker Tensor II.

Synthesis method

Synthesis of [CuCe L(Cl_4-bdc)$_{0.5}$(H_2O)$_2$·(H_2O)$_6$]$_n$:

A mixture of $CuCl_2·2H_2O$ (140 mg), $Ce(NO_3)_3·6H_2O$ (180 mg), 1H-pyrazole-3,4,5-tricarboxylic acid (35 mg) and Cl_4-bdc (60 mg，Cl_4-bdc = 2,3,5,6-tetrachloroterephthalate), KOH (14 mg), and H_2O (12.5 mL) were sealed in a 25 mL Teflon-lined stainless steel autoclave. The autoclave was heated to 120 °C for 72 h under autogenous pressure without disturbance and cooled slowly to room temperature with a rate of 2 °C·h^{-1}. Blue block crystals were formed and collected by filtration, washed with EtOH and dried in air. Yield: 30% (based on 1H-pyrazole-3,4,5-tricarboxylic acid). FT-IR (cm^{-1}): 1640 (vs), 1586 (vs), 1507 (s), 1438 (s), 1380 (s), 1348 (m), 1306 (m), 1147 (m), 847 (m), 631 (m).

X-ray Crystallography

X-ray single-crystal diffraction datum for the crystal of **1** was collected with the Rigaku Xtlab-Min diffractometer at 293(2) K with Mo-Kα radiation (λ = 0.71073 Å) by ω scan mode. The program CrysAlisPro 1.171.39.7e[1] was used for the integration of the diffraction profiles. The structure was determined by the intrinsic phasing method using ShelXT[2] and refined by full-matrix least-squares methods using ShelXL[3] with Olex2.[4] The crystal data of the MOF are shown in Table S1, and the selected bond lengths and angles are given in Table S2.

Gas adsorption measurement

Gas adsorption isotherms were performed by using Micromeritics ASAP 2020 PLUS HD88 instrument. In a typical measurement, 0.3 g of the crystal sample was degassed under vacuum at 146 °C for 12 h prior to measurements. The testing temperatures, 273 and 298 K were maintained by ice-water bath and water bath at constant temperature, respectively.

Breakthrough test

The breakthrough tests were measured by the Multi-component Adsorption Breakthrough Curve Analyzer (BSD-MAB). Firstly, the activated sample was extruded by the tablet machine, then ground and sieved by the 40-60 screen mesh, from which it was put into the tube（φ 6 mm × 60 mm）. Next, the He was pumped into the adsorption bed for 2 h to expel others gas. Finally, the CH_4/N_2 binary mixed gases (50% : 50%) were passed through the adsorption bed, respectively. The gas concentrations of effluents were measured by on-line mass spectrometry.

Calculation of isosteric heat of adsorption

Isosteric heat of adsorption (Q_{st}) was derived from the adsorption data using the viral equation[5]:

$$In(P) = In(N) + \frac{1}{T}\sum_{i=0}^{m} a_i N^i + \sum_{j=0}^{n} b_j N^j \quad \text{(S1)}$$

where P is pressure, N is the amount adsorbed at pressure P, T is temperature, m and n determine the number of terms required to adequately describe the isotherm, and a_i

and b_j are empirical parameters.

Theoretical calculations

DFT calculations were carried out using the CP2K code.[6] All calculations employed a mixed Gaussian and planewave basis sets. Core electrons were represented with norm-conserving Goedecker-Teter-Hutter pseudopotentials,[7-9] and the valence electron wavefunction was expanded in a double-zeta basis set with polarization functions[10] along with an auxiliary plane wave basis set with an energy cutoff of 360 Ry. The generalized gradient approximation exchange-correlation functional of Perdew, Burke, and Enzerhof (PBE)[11] was used. Each configuration was optimized with the Broyden-Fletcher-Goldfarb-Shanno (BGFS) algorithm with SCF convergence criteria of 1.0×10^{-8} au. To compensate the long-range van der Waals dispersion interaction between the adsorbate and **1**, the DFT-D3 scheme[12] with an empirical damped potential term was added into the energies obtained from exchange-correlation functional in all calculations.

The adsorption energy between the adsorbate and the **1** can be calculated using the following equation:

$$\Delta E = E_{adsorbate@MOF} - E_{MOF} - E_{adsorbate} \quad \text{(S2)}$$

In Eq. (S2), $E_{adsorbate@MOF}$ and E_{MOF} represent the total energies of **1** with and without adsorbate, respectively. $E_{adsorbate}$ is the total energy of the adsorbate. According to this equation, a negative adsorption energy corresponds a stable adsorption structure.

Ideal adsorption solution theory (IAST) calculations

The CH_4 and N_2 adsorption isotherms were fitted by a dual-site Langmuir model (equation S3)

$$q = q_A + q_B = \frac{q_{sat,\,A} b_A p}{1 + b_A p} + \frac{q_{sat,\,B} b_B p}{1 + b_B p} \quad \text{(S3)}$$

where q is the amount of adsorbate, q_{sat} is the saturation amount, b is the Langmuir parameter, p is the bulk gas phase pressure, A and B refer to two different sites.

The ideal adsorbed solution theory (IAST) selectivity calculations were carried out to assume CH_4/N_2 gas mixtures which were derived by using the equation S4[13]:

$$S = \frac{q_1 p_2}{q_2 p_1} \quad \text{(S4)}$$

where S represents adsorption selectivity of 1 and 2 components; q_1 and q_2 are the gas adsorption capacities of 1 and 2 components, the p_1 and p_2 are gas molar the partial pressure of 1 and 2 component, respectively.

Table S1 The crystallographic parameters of **1**

	1
Empirical formula	$C_{10}H_{16}CeCl_2CuN_2O_{16}$
Formula weight	694.81
Temperature/K	293(2)
Crystal system	triclinic
Space group	$P\bar{1}$
a/Å	7.0146(3)
b/Å	11.4515(6)
c/Å	13.7995(6)
α/°	95.556(4)
β/°	98.767(4)
γ/°	98.440(4)
Volume/Å^3	1075.58(9)
Z	2
ρ_{calc} g/cm^3	2.145
μ/mm^{-1}	3.407
F(000)	678
Reflections collected	5760
Independent reflections	3791
Data/restraints/parameters	3791/0/309
Goodness-of-fit on F^2	0.505
R_1 [I>=2σ(I)][a]	0.0437
R_1 [all data][b]	0.0547
wR_2 [I>=2σ(I)][a]	0.1114
wR_2 [all data][b]	0.1219

[a]$R_1 = \sum ||F_o| - |F_c|| / \sum |F_o|$; [b]$wR_2 = [\sum [w(F_o^2 - F_c^2)^2] / \sum w(F_o^2)^2]^{1/2}$.

TableS2 The bonds lengths (Å) for **1**

Ce1-O6^{i}	2.602(4)	Ce1-O1	2.470(5)
Ce1-O6^{ii}	2.557(5)	Ce1-O9	2.500(6)
Ce1-O5^{i}	2.715(4)	Cu1-O3	2.004(5)
Ce1-O5	2.443(5)	Cu1-O8^{iii}	1.995(5)
Ce1-O4	2.429(4)	Cu1-N2^{iii}	1.933(6)
Ce1-O7^{ii}	2.460(5)	Cu1-N1	1.931(6)
Ce1-O2^{i}	2.505(5)	Cu1-O10	2.290(7)

Symmetry codes: (i) 2-X,1-Y,1-Z; (ii) 1+X,+Y,+Z; (iii) 1-X,1-Y,-Z.

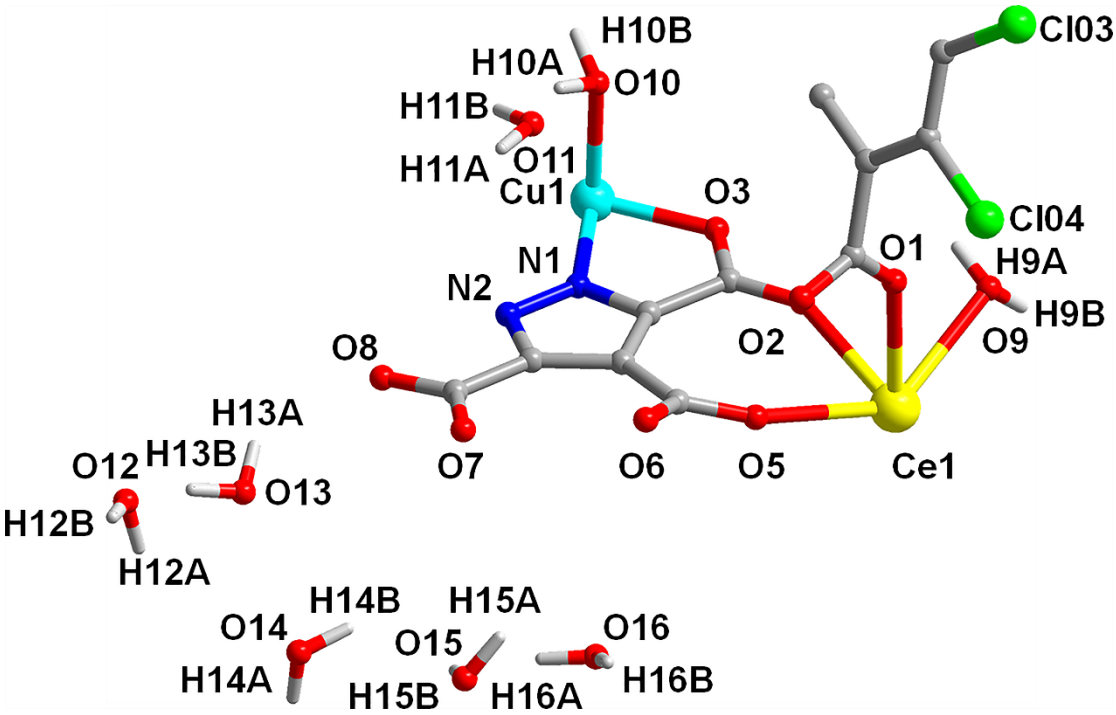

Fig. S1 Asymmetric unit cell diagram.

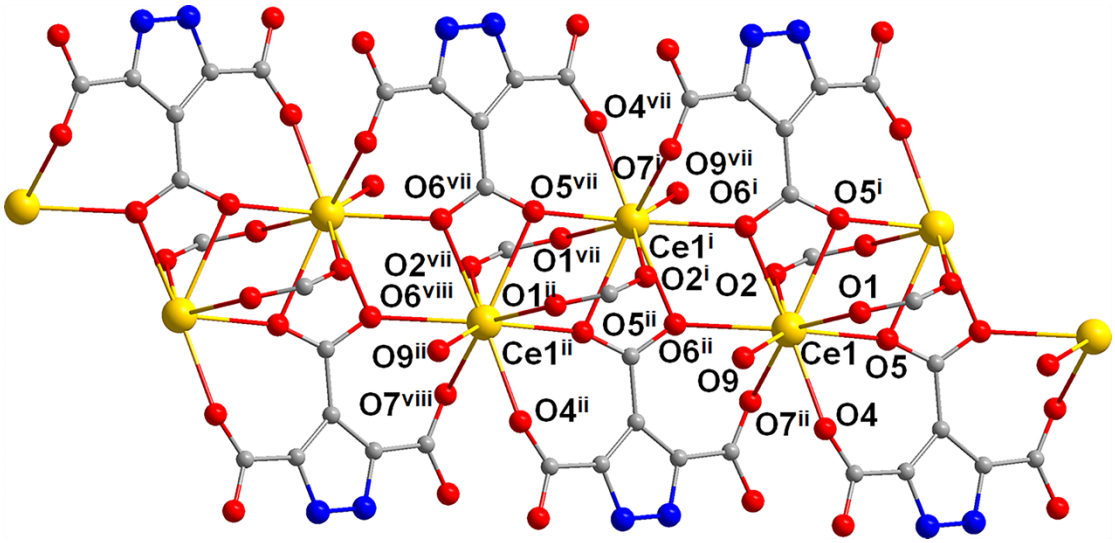

Fig. S2 Ce coordination chain in **1**. Symmetry codes: [i] 2-X,1-Y,1-Z; [ii] 1+X,+Y,+Z; [iii] 1-X,1-Y,-Z; [iv] -1+X,+Y,+Z; [v] 2-X,2-Y,1-Z; [vi] +X,1+Y,+Z; [vii] 3-X,1-Y,1-Z; [viii] 2+X,+Y,+Z; [ix] -1+X,+Y,-1+Z; [x] 2-X,1-Y,-Z.

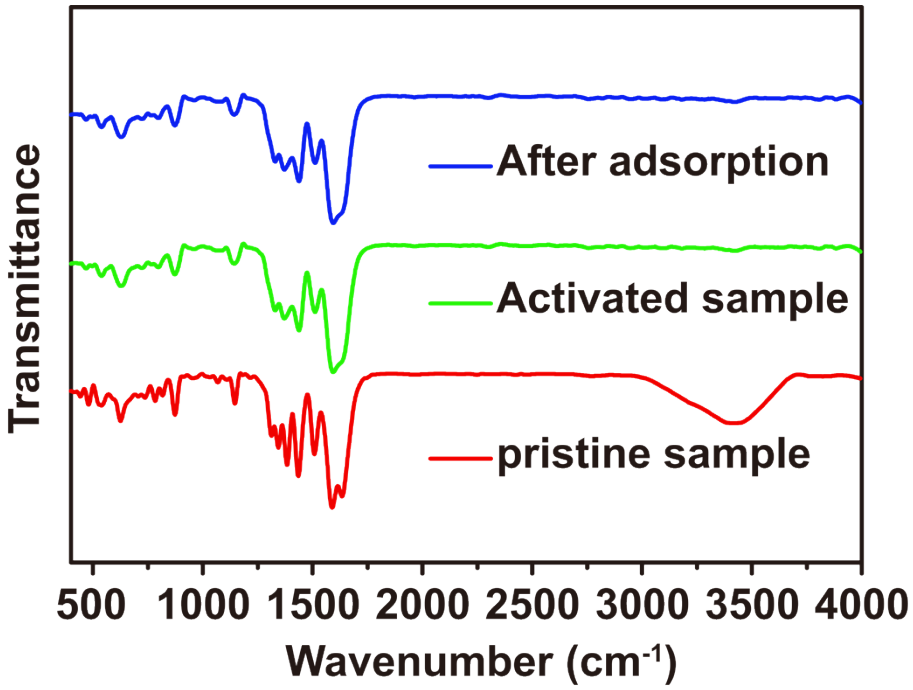

Fig. S3 FT-IR spectra of **1** before activation process (red), after activation process (green) and after adsorption (blue).

After activation process, the peak in the range from 3100 to 3700 cm-1 which refer to the

stretching vibration modes of the O-H bonds has disappeared which suggest that almost all water molecules have been removed under activating process. Besides, after activation process and adsorption experiment, the spectra matched well with the pristine sample which indicate the framework can keep intact in these processes. some important peaks have been listed: the peak at 1640 cm^{-1} and 1586 cm^{-1} are ascribed to the stretching vibration of the C=O and C=N bonds in Carboxyl group and pyrazole rings, respectively, while the peak at 1512 cm^{-1} refer to the stretching vibration of the C=C bonds in benzene rings, the peak at 1375 cm^{-1} refer to the stretching vibration of the C-Cl bonds in Cl_4-bdc.

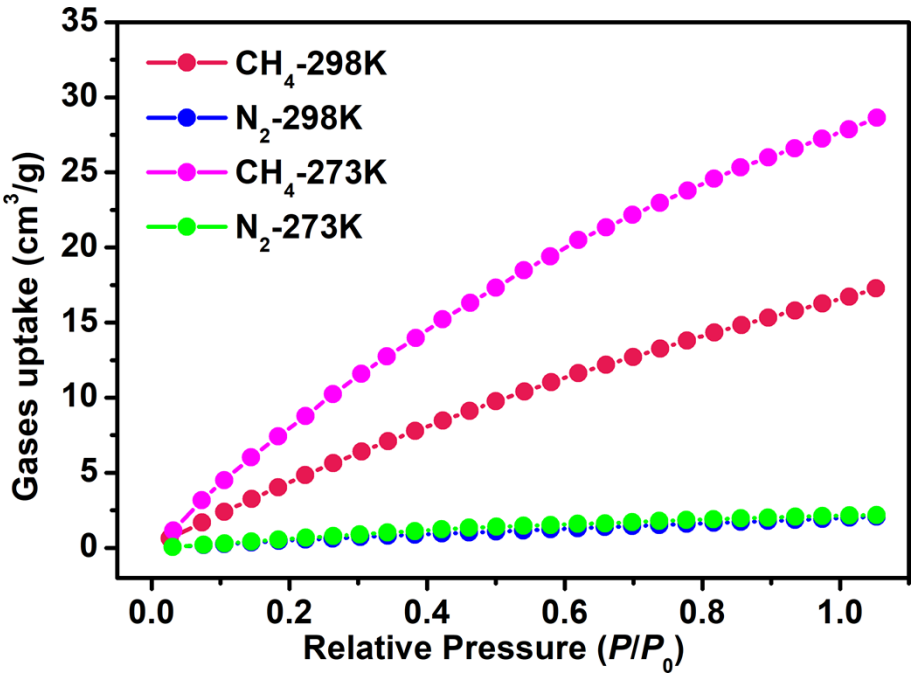

Fig. S4 The mass adsorption capacity of **1** for CH_4 and N_2 at 273 K and 298 K, respectively.

Table S3. The gas adsorption and separation performances of various porous materials from reported results.

Adsorbents	CH_4/N_2 Selectivity	CH_4 capacity $cm^3(STP)/cm^3$	Q_{st}^0 (kJ/mol)		Refs.
			CH_4	N_2	
MOF-type materials					
Al-CDC	13.1[a]	41.86	27.5	18.6	13
$Co_3(C_4O_4)_2(OH)_2$	12.5[a]	19.81	25.1	18.1	14
STAM-1	11.1[a]	19.64	20.0	15.0	15
ATC-Cu	9.7[a]	68.33	26.8	16.0	16
ROD-8	9.1[a]	21.89	16.7		17
MOF-888	8.4[a]	11.27	26.0	22.0	18
$Cu(INA)_2$	8.3[b]	30.37	17.5		19
MOF-891	7.8[a]	42.22	22.0	21.0	18
$Ni(OAc)_2L$	7.0[a]	20.92	26.7	20.0	20
MOF-890	7.0[a]	32.18	23.0	19.0	18
MOF-889	6.4[a]	32.14	22.0	19.0	18
Ni-HKUST-1	5.1[a]	0.07			21
Al-BDC	3.6[b]	11.74	18.7		19
This work	13.32[a]	28.41	13.2		This work

[a] Predicted by IAST.

[b] Calculated from the ratio of Henry constants.

References:

[1] *CrysAlisPro 1.171.39.7e, Empirical Absorption Correction Using Spherical Harmonics, Implemented in SCALE3 ABSPACK Scaling Algorithm;* Rigaku Oxford Diffraction, 2015.

[2] G. M. Sheldrick, SHELXT-integrated space-group and crystal-structure determination, *Crystallogr. Sect. A: Found. Adv.*, 2015, **71**, 3-8.

[3] G. M. Sheldrick, Crystal structure refinement with SHELXL, *Acta Crystallogr. Sect. C: Struct. Chem.*, 2015, **71**, 3-8.

[4] O. V. Dolomanov, L. J. Bourhis, R. J. Gildea, J. A. K. Howard and H. Puschmann, OLEX2: a complete structure solution, refinement and analysis program, *J. Appl. Crystallogr.*, 2009, **42**, 339-341.

[5] M. G. Rabbani, A. K. Sekizkardes, O. M. El-Kadri, B. R. Kaafarani and H. M. El-Kaderi, Pyrene-directed growth of nanoporous benzimidazole-linked nanofibers and their application to selective CO_2 capture and separation, *J. Mater. Chem.*, 2012, **22**, 25409-25417.

[6] J. VandeVondele, M. Krack, F. Mohamed, M. Parrinello, T. Chassaing and J. Hutter, Quickstep: fast and accurate density functional calculations using a mixed Gaussian and plane waves approach, *Comput. Phys. Commun.*, 2005, **167**, 103-128.

[7] S. Goedecker, M. Teter and J. Hutter, Separable dual-space gaussian pseudopotentials. *Phys. Rev. B*, 1996, **54**, 1703-1710.

[8] C. Hartwigsen, S. Goedecker and J. Hutter, Relativistic separable dual-space gaussian pseudopotentials from H to Rn, *Phys. Rev. B*, 1998, **58**, 3641-3662.

[9] M. Krack and M. Parrinello, All-electron ab-initio molecular dynamics. *Phys. Chem. Chem. Phys.*, 2000, **2**, 2105-2112.

[10] J. VandeVondele and J. Hutter, Gaussian basis sets for accurate calculations on molecular systems in gas and condensed phases, *J. Chem. Phys.*, 2007, **127**, 114105.

[11] J. P. Perdew, K. Burke, M. Ernzerhof, Generalized gradient approximation made simple. *Phys. Rev. Lett.*, 1996, **77**, 3865-3868.

[12] S. Grimme, J. Antony, S. Ehrlich and H. Krieg, A consistent and accurate ab initio parametrization of density functional dispersion correction (DFT-D) for the 94 elements H-Pu, *J. Chem. Phys.*, 2010, **132**, 154104.

[13] M. Chang, Y. Zhao, D. Liu, J. Yang, J. Li and C. Zhong, Methane-trapping metal-organic frameworks with an aliphatic ligand for efficient CH_4/N_2 separation, *Sustainable Energy Fuels*, 2020, **4**, 138-142.

[14] L. Li, L. Yang, J. Wang, Z. Zhang, Q. Yang, Y. Yang, Q. Ren, Z. Bao, Highly efficient separation of methane from nitrogen on a squarate-based metal-organic framework, *AIChE J.*, 2018, **64**, 3681-3689.

[15] M. Chang, Y. Zhao, Q. Yang, D. Liu, Microporous metal-organic frameworks with hydrophilic and hydrophobic pores for efficient separation of CH_4/N_2 mixture, *ACS Omega*, 2019, **4**, 14511-14516.

[16] Z. Niu, X. Cui, T. Pham, P. Lan, H. Xing, K. A. Forrest, L. Wojtas, B. Space, S. Ma, A metal-organic framework based methane nano-trap for the capture of coal-mine methane, *Angew. Chem. Int. Ed.*, 2019, **58**, 10138-10141.

[17] R. Li, M. Li, X. Zhou, S. W. Ng, M. O'Keeffe, D. Li, ROD-8, a rod MOF with a pyrene-cored tetracarboxylate linker: framework disorder, derived nets and selective gas adsorption, *CrystEngComm*, 2014, **16**, 6291-6295.

[18] P. T. K. Nguyen, H T. D. Nguyen, H. Q. Pham, J. Kim, K. E. Cordova, H. Furukawa, Synthesis and selective CO_2 capture properties of a series of hexatopic linker-based metal-organic frameworks, *Inorg. Chem.*, 2015, **54**, 10065-10072.

[19] J. Hu, T. Sun, X. Liu, Y. Guo, S. Wang, Separation of CH_4/N_2 mixtures in metal-organic frameworks with 1D micro-channels, *RSC Adv.*,2016, **6**, 64039-64046.

[20] C. Kivi, B. Gelfand, H. Dureckova, H. Ho, C. Ma, G. Shimizu, T. Woo, D. Song, 3D porous metal-organic framework for selective adsorption of methane over dinitrogen under ambient pressure, *Chem. Commun.*,2018, **54**, 14104-14107.

[21] X. Jia, N. Yuan, L. Wang, J. Yang, J. Li, $(CH_3)_2$ NH-Assisted Synthesis of High-Purity Ni-HKUST-1 for the Adsorption of CO_2, CH_4, and N_2, *Eur. J. Inorg. Chem.*, 2018, **8**, 1047-1052.